Traversed Graph Representation for Sparse Encoding of Macro-Reentrant Tachycardia

Mihaela Constantinescu[1]([✉]), Su-Lin Lee[1], Sabine Ernst[2],
and Guang-Zhong Yang[1]

[1] The Hamlyn Centre for Robotic Surgery, Imperial College London, London, UK
`mihaela.constantinescu12@imperial.ac.uk`
[2] The Royal Brompton and Harefield Hospital, London, UK

Abstract. Macro-reentrant atrial and ventricular tachycardias originate from additional circuits in which the activation of the cardiac chambers follows a high-frequency rotating pattern. The macro-reentrant circuit can be interrupted by targeted radiofrequency energy delivery with a linear lesion transecting the pathway. The choice of the optimal ablation site is determined by the operator's experience, thus limiting the procedure success, increasing its duration and also unnecessarily extending the ablated tissue area in the case of incorrect ablation target estimation. In this paper, an algorithm for automatic intraoperative detection of the tachycardia reentry path is proposed by modelling the propagation as a graph traverse problem. Moreover, the optimal ablation point where the path should be transected is computed. Finally, the proposed method is applied to sparse electroanatomical data to demonstrate its use when undersampled mapping occurs. Thirteen electroanatomical maps of right ventricle and right and left atrium tachycardias from patients treated for congenital heart disease were analysed retrospectively in this study, with prediction accuracy tested against the recorded ablation sites and arrhythmia termination points.

1 Introduction

In recent years, catheter ablation of cardiac arrhythmias has moved from ablation of 'simple' substrates like accessory pathways to more complex arrhythmias such as atrial or ventricular tachycardia or fibrillation. Even patients with complex congenital heart disease (CHD) that may present with a very unusual cardiac anatomy can now be candidates for catheter ablation procedures. Merging pre-procedural 3D image data with the 3D electroanatomy has provided a very valuable tool to improve ablation outcomes even during longterm follow-up.

The state-of-the-art in intraoperative guidance for mapping and ablating tachycardias in CHD includes CARTO (Biosense Webster, Bar Diamond, CA, US). After vascular access into the cardiac chamber, the mapping catheter is moved in contact with the endocardial wall in order to generate the spatial information, i.e. the fast anatomical map (FAM), and also acquire sparse electrical data at specifically selected points on the FAM. The electrical parameters

include unipolar and bipolar voltage and local activation times (LAT). With each point acquisition, CARTO interpolates the electrical parameters across the FAM using a preset distance threshold. From the LAT map, CARTO is able to simulate the activation wave based on a sequential plot of activation time geodesics. Apart from CARTO, a second widely used electroanatomical mapping system is EnSite NavX (St. Jude Medical, St. Paul, MN, US), which outputs the same activation time and voltage maps as CARTO, but employs a different technology. Despite the advances in these two systems, establishing the path of fastest conduction, i.e. the main ectopic propagation circuit, and correlating it with the location of fibrotic tissue shown on the bipolar voltage map are still operator-dependent skills.

Intra-operatively, the electrophysiologists guide themselves in locating the circuit by circuit entrainment mapping. They measure the post pacing interval at the reset of the tachycardia to see if the circuit was entered successfully. Naturally, with increasing numbers of mapping and pacing points, the activation and voltage amplitude maps become more accurate. However, there is a trade-off between mapping time and resolution. Moreover, if the ablation site is, by error or misinterpretation of the mapping data, far from the conduction path, repeated energy delivery will be required, causing more tissue damage than necessary. Successful ablation is declared if the mapped tachycardia is terminated during energy delivery and no longer inducible.

In order to understand the underlying mechanisms of macro-reentrant tachycardias, different electrophysiological models have been proposed for simulation. These models are meant to replace to some extent the more expensive electroanatomical mapping systems. They use general electrical wave propagation principles applied to the cardiac tissue and anatomy and personalised with electromechanical parameters from preoperative imaging. Although the well-established CARTO and EnSite technologies are preferred in clinical practice, the electroanatomical models can also provide the cardiologists with activation time maps and potentially voltage information. Among the least computationally expensive frameworks are the eikonal model for conduction parameter estimation at macro-scale [1,2], but also simplified biophysical ionic channel models [3] or mono-domain models such as Lattice-Boltzmann [4]. Fast Marching, an adaptation of the graph traverse Dijkstra algorithm, is typically used to solve the differential equations in these models. The solution of these equations can be mapped on 3D anatomy in order to mimic the information output of electroanatomical mapping systems. Alternatives to these classical biophysical approaches are the models of propagation in cellular automata [5] and the estimation of pathways as a minimal cost graph traverse formulation [6], the latter having been used for qualitative identification of the normal conduction along the Purkinje fibres.

This paper proposes a novel approach for the detection of tachycardia propagation path based on graph traverse theory by using the mapping data directly and without the need for simulation or electroanatomical model fitting. Furthermore, the point in the circuit of the highest termination probability was computed. The algorithms were tested for repeatability in sparse mapping

conditions when fewer points are acquired. The proposed method was validated with data from 13 patients with previous CHD surgery and suffering from atrial or ventricular reentrant tachycardias.

2   Methods

2.1   Data Acquisition

CARTO 3 studies of macro-reentrant right ventricular and left and right atrial tachycardia were collected – 4 right ventricles, 6 right atria, 2 left atria, 1 total cavopulmonary connection (TCPC). Each study contained a 3D endocardial surface of the cardiac chamber, with a corresponding set of LATs, bipolar voltages, and unipolar voltages for each surface vertex. The anatomical meshes were smoothed with Poisson reconstruction, threshold set as the default 6, in Mesh-Lab [7]. The electrical data at the new vertices were interpolated linearly from the values on the original meshes. The latest and earliest activation times with respect to the end-diastolic ECG peak (R peak) were extracted. The input data required by the proposed method is independent of the CARTO system, as long as the electroanatomical information can be recovered with another technology, e.g. EnSite, or modelled using any cardiac activation principles.

2.2   Macro-Reentrant Circuit Reconstruction

For macro-reentrant circuit reconstruction, the shortest geodesic path between the earliest and the latest activation vertices was computed. The mesh edges were used as graph edges and the vertices as nodes. The edges were weighted with the propagation speed between the vertices that they connected, multiplied by the means of the bipolar and unipolar voltage amplitudes at the two vertices (Eq. 1).

$$w_{i,j} = \frac{d_{i,j}}{|\mathrm{LAT}_i - \mathrm{LAT}_j|} \cdot \frac{V_{\mathrm{uni},i} + V_{\mathrm{uni},j}}{2} \cdot \frac{V_{\mathrm{bi},i} + V_{\mathrm{bi},j}}{2} \tag{1}$$

The variable $w_{i,j}$ is the weight of the edge connecting vertex i to vertex j, each with activation times LAT_i and LAT_j, unipolar voltage amplitudes $V_{\mathrm{uni},i}$ and $V_{\mathrm{uni},j}$, and bipolar voltage amplitudes $V_{\mathrm{bi},i}$ and $V_{\mathrm{bi},j}$. The propagation speed between the neighbouring vertices i and j was computed from the Euclidean distance $d_{i,j}$. The product of mean voltage amplitudes modelled the energy of the wave traversing that part of the tissue, dependent on the tissue conductivity. This modulated the path to avoid crossing areas of surgical scars, which have low conductivity. Finally, Dijkstra's algorithm was applied [8].

Due to the limitations of the interpolation algorithm in CARTO, the earliest and latest activation points may not directly coincide, leaving a strip of artificially interpolated LATs (Fig. 1). Also in some cases, the incomplete geometry of the endocardial chamber caused the activation circuit to be represented only partially. The remaining gap was closed with a new application of the Dijkstra algorithm on the complementary path, which was forced to pass through the vertex opposite to the centre of the path found in the first Dijkstra run.

2.3 Tachycardia Termination Point Detection

The electrical features of typical tachycardia points were learned and tested in a leave-one-out fashion. For each of the 13 studies, the triplets of LAT, bipolar voltages, and unipolar voltages of the points along the path were normalised and concatenated. The LATs were a measure of position of the termination points along the parameterised path running from earliest to latest activation; the voltages were a measure of tissue fibrosis. Each study was left out in turn from the full set of 13. The points on the remaining 12 paths were fed as a training set into an adapted version of a random subsampling boosting classifier (RUSBoost, presented in [9] and adapted as in Algorithm 1).

The labels of the training set were exported from CARTO and projected onto the paths, in order to distinguish between the features of the two classes, ablation points and regular points. The learner predicted the labels of the path points on the test case. RUSBoost was deemed the most adequate classification method given the imbalanced number of termination points compared to the other points on the path.

Data:
- $(y_{\text{train},i}, \text{LAT}_{\text{train},i}, \text{bi}_{\text{train},i}, \text{uni}_{\text{train},i})$, $i = \overline{1, n_{\text{train}}}$ and $y_{\text{train},i} \in \{0, 1\}$, where 0 denotes regular path point and 1 termination point, as marked in CARTO
- number of termination points is significantly lower than the number of regular path points, i.e. $n_1 \ll n_0$
- $(\text{LAT}_{\text{test},i}, \text{bi}_{\text{test},i}, \text{uni}_{\text{test},i})$, $i = \overline{1, n_{\text{test}}}$
- weak learner, which does not necessarily yield a good initial classification.

Initialization: $w_{1,i} = \frac{1}{n_{\text{train}}}, i = \overline{1, n_{\text{train}}}$, where $w_{k,i}$ is the weight of sample i in iteration k;
while *preset number of iterations not reached* **do**

1. subsample from the full set using the weights $w_{k,i}$, $i = \overline{1, n_{\text{train}}}$;
2. feed the subset and the weights to the learner;
3. learner estimates the labels of the training data;
4. update the weights with the classification error;

end
Result: $y_{\text{test},i} = 0$ or $y_{\text{test},i} = 1$, $p(y_{\text{test},i} = 1)$, and $p(y_{\text{test},i} \neq 1)$, where $i = \overline{1, n_{\text{test}}}$

Algorithm 1. RUSBoost classification algorithm for detection of most probable point of tachycardia termination

2.4 Subsampling of Electroanatomical Maps

Electrical Data Interpolation. In order to test how the circuit reconstruction and the termination point detection perform on sparse electroanatomical data, subsampling of the original maps was performed. The electrical values of every vertex in the sparse maps were obtained through a two-step interpolation and

threshold filling algorithm, tuned to mimic the online interpolation of CARTO when new electroanatomical data is acquired.

In the first step, for every vertex, only the mapping points within a 12 mm radius were taken into consideration. The value at that vertex was either that of the mapping points, if it coincided, or the mean of the values of all mapping points within 12 mm, weighted inversely with the distance from the vertex. In the second step, the vertices which did not have any mapping points to meet the proximity threshold were given the value of their closest vertex with an assigned value from the interpolation step. The value of 12 mm was set by trial and error to best match the CARTO ground truth. A qualitative comparison can be made between the figures in Table 2 and the original mesh in Fig. 1.

Iterative Cluster Subsampling. The original mapping points were clustered around 5 centroids computed with the k-means method and approximated by the closest mapping point in the cluster according to the Cartesian distance. The 5 centroids were ordered using a greedy search with respect to their marginal information, which is explained in the next paragraphs.

Given the full set of mapping points P_0, from which the ground-truth electroanatomical map was built, and a subset $P \subset P_0$, the map reconstruction accuracy when using subset P for interpolation can be computed as the inverse of the error

$$\varepsilon_{P \sim P_0} = \frac{1}{3} \sum_{i \in \{\text{LAT,uni,bi}\}} \frac{1}{j} \sum_{j=1}^{n_V} \frac{|f_{i,j,P} - f_{i,j,P_0}|}{\max_{i,j} f_{i,j,P_0} - \min_{i,j} f_{i,j,P_0}}. \tag{2}$$

The anatomy is in both cases a 3D surface of n_V vertices. The value $f_{i,j}, i \in \{\text{LAT,uni,bi}\}$, is either the LAT, unipolar voltage (uni), or bipolar (bi) voltage at vertex j. For each vertex, the difference in electroanatomical values was scaled with reference to the P_0 map. The marginal information of a mapping point can be defined as the difference in map accuracy between two maps constructed with and without that particular point. The adapted greedy search for ordering the centroids according to their marginal information is presented in Algorithm 2.

The path reconstruction and termination point detection were run in 5 iterations, where in each iteration a new cluster of points was added to interpolate the colour maps.

3   Results

3.1   Macro-Reentrant Circuit Reconstruction

For each of the 13 cases, the graph was built with the FAM vertices and edges. The forward circuit was computed using Matlab's implementation of the Dijkstra algorithm with weights as in Eq. 1. Figure 1 shows qualitative results on a right ventricle and on left and right atria. The CARTO ablation, circuit entrainment, and termination points are displayed as reference points of the ground-truth propagation path detected intraoperatively. The dense bipolar voltage maps were

Data:
- P_0 full set of mapping points;
- f_{i,j,P_0}, $i \in \{LAT, uni, bi\}$, $j = \overline{1, n_V}$, electrical features of all vertices for the map computed with the points in P_0
- vertex indices of the 5 centroids

Initialization: $c_1 = \arg\min_k \varepsilon_{(P_0 - \{k\}) \sim P_0}$, $k = \overline{1, 5}$;
while $i <=$ *number of clusters - 1* **do**

    1. interpolate for $f_{i,j,\{c_{\overline{1,i}}\}}$ and $f_{i,j,(\{c_{\overline{1,i}}\} \cup \{k\})}$, where $k = \overline{1,5} - \{c_{\overline{1,i}}\}$;

    2. $c_{i+1} = \arg\max_k |\varepsilon_{\{c_{\overline{1,i}}\} \sim P_0} - \varepsilon_{(\{c_{\overline{1,i}}\} \cup \{k\}) \sim P_0}|$;

    3. $i = i + 1$;

end
Result: **c**, decreasing order of centroid marginal information

Algorithm 2. Ordering of the cluster centroids according to their marginal information added to the electroanatomical map

thresholded at $0.5\,\mathrm{mV}$, a value commonly used in the EP literature for ventricular scar segmentation in electroanatomic data. The third row of results, displayed on top of the scar maps, shows that the calculation of propagation paths avoids the crossing of scars, according to the edge weights in Eq. 1.

Several qualitative observations can be made from the results shown in Fig. 1. Firstly, there was a good correlation between the LAT geodesics and the computed path perpendicular to them. Secondly, the paths were modulated by the presence of surgical scar, encoded by the bipolar voltage amplitude at each vertex. The perpendicularity of the paths to the LAT geodesics is ensured by the core principle of shortest path in the Dijkstra algorithm.

Table 1 shows a quantitative analysis of both tachycardia circuit detection and termination point learning. Assuming that all critical points labelled intraoperatively and imported from CARTO, i.e. circuit entrainment, ablation, and final tachycardia termination points, lie on the true wave propagation path, an accuracy measure was defined as the distance between this ground-truth and the computed path, namely the mean distance to CARTO points. The average of $16.36\,\mathrm{mm}$ was comparable to the range of tip instability of the ablation catheter ($12\,\mathrm{mm}$), as recorded by the electromagnetic sensors in the CARTO framework.

3.2   Tachycardia Termination Point Detection

Several measures were defined to assess the method's performance in this step: the accuracy, sensitivity, and specificity, all of which quantified the ability to distinguish a regular path point from an critical point on the path. A critical point is either an ablation, a termination, or a circuit entrainment point as labelled and exported from CARTO. A critical path point is the projection of a critical point onto the tachycardia path reconstructed in the first step of the method.
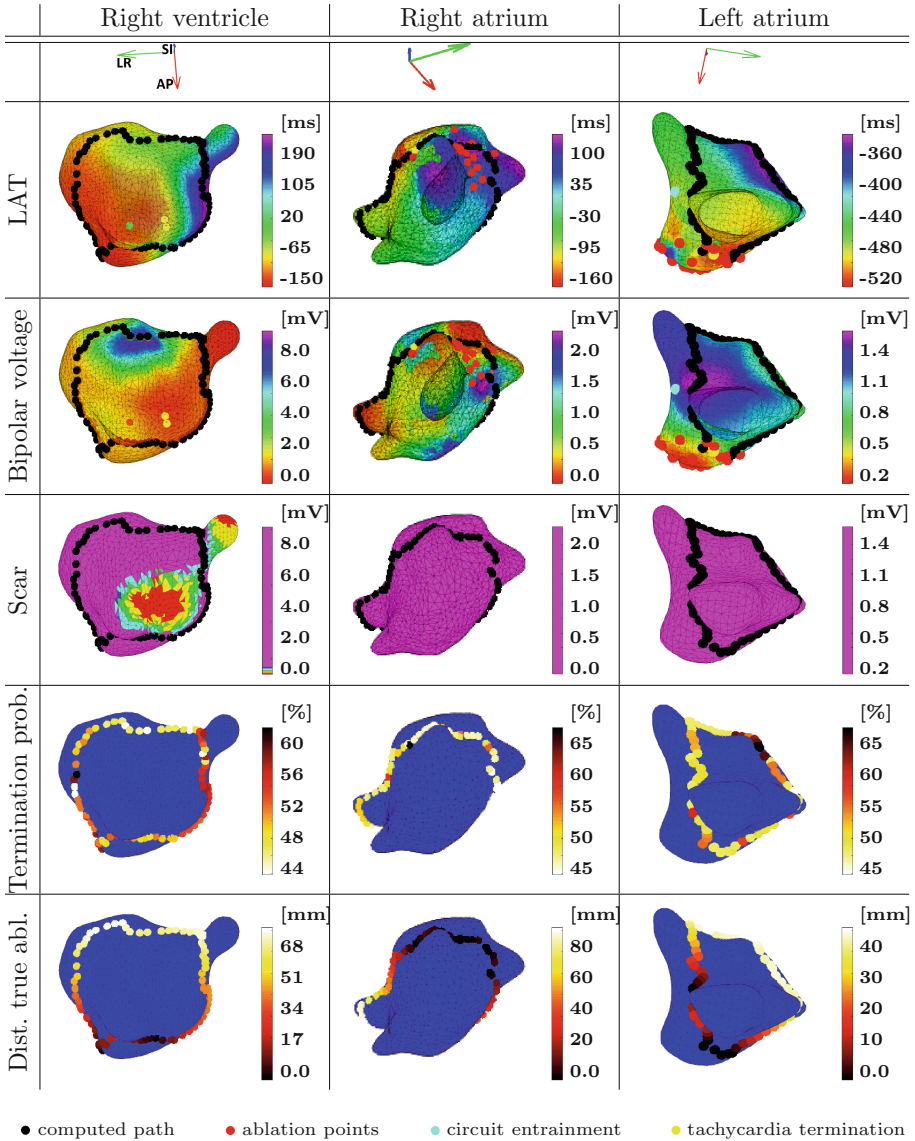
Fig. 1. Tachycardia propagation path for average right and left atria and for an average right ventricle. The panels show from top to bottom the LAT, bipolar voltage, and scar maps, the probability of tachycardia termination at each point along the path, and the distance of the computed termination points from the closest ground-truth ablation. AP – antero-posterior axis, LR – left-right axis, SI – supero-inferior axis.

Apart from the relative performance measures, the average minimal distance to the critical path points was computed. These points were all considered the ground-truth termination points, as it was difficult to assess which of them led

Table 1. Distance of computed propagation path from critical points, i.e. ablation, termination and circuit entrainment points marked in CARTO, i.e. critical CARTO points; characteristics of the tachycardia termination point classifier and distance of the point with the highest computed probability of termination from actual CARTO critical points.

	RV	RA	LA	TCPC	Mean
Mean distance to CARTO points [mm]	22.25	14.09	13.98	3.77	16.36
Standard deviation [mm]	13.05	12.16	6.98	3.53	12.03
Accuracy [%]	59.26	71.59	72.37	79.10	68.49
Specificity [%]	62.07	75.64	75.40	82.26	71.94
Sensitivity [%]	38.54	33.06	47.62	40.00	37.52
Avg. min. dist. to CARTO points [mm]	0.00	2.84	0.00	2.46	1.52
Standard deviation [mm]	0.00	4.19	0.00	0.00	3.06

to the tachycardia termination. For every path point, the closest critical path point was found. This distance was then averaged over all path points.

The leave-one-out ensemble learning yielded a mean accuracy of 68.49 % in detecting critical points along the propagation path (Table 1). The points with a termination probability over 50 % lay within 1.52 mm from their closest critical path point. The lowest error was recorded in RV and LA, for which all computed termination points matched a ground-truth critical point (0.00 entries in the table). The computed tachycardia termination was colour-coded to emphasize the points of highest probability. Table 1 averages the results of both circuit reconstruction and critical point detection for each type of cardiac chamber.
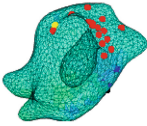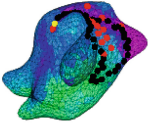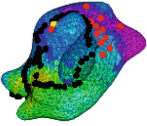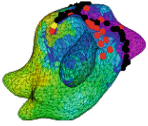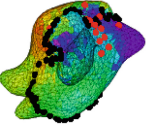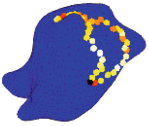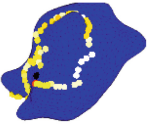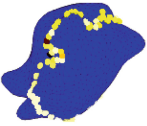
3.3   Performance on Subsampled Electroanatomical Maps

The path reconstruction and termination point detection algorithms were applied on 5 iterations of subsampling in each study. Results for a right atrium are presented in Table 2 which shows how the tachycardia circuit was re-shaped with the addition of new mapping points and how the classification algorithm changed its output.

4   Discussion and Conclusion

In this paper, a traversed graph representation for sparse encoding of macro-reentrant tachycardia was presented. In addition to good qualitative correlation with the geodesics in the LAT map, the Cartesian distance to the true termination and circuit entrainment points also support the applicability of the algorithm. The observed error in this study was primarily caused by the interpolation limitations in CARTO, a system error which could be alleviated with the use of another electroanatomical mapping system or in a simulated cardiac activation software.

Table 2. Sequence of propagation path reconstruction for the right atrium in Fig. 1 (upper table) and average over all cases (lower table). The points were added in decreasing order of their k-mean cluster centroid's marginal information value. A – accuracy [%], Sp – specificity [%], Se – sensitivity [%], d – minimal distance to CARTO ablation [mm], D – average distance to CARTO critical points, assumed on the ground-truth path [mm], σ – standard deviation of the distances to CARTO critical points [mm].

	Iteration #1	Iteration #2	Iteration #3	Iteration #4	Iteration #5
LAT					
Termination					
D	52.81	2.78	11.12	3.85	6.71
σ	7.67	5.17	5.17	5.17	6.71
A	73.33	42.22	50.63	35.21	60.27
Sp	78.57	37.84	50.00	37.50	62.69
Se	0.00	62.50	60.00	14.29	33.33
d	52.12	0.00	2.22	0.00	3.59

● computed path   ● ablation points   ● circuit entrainment   ● tachycardia termination

	Iteration #1	Iteration #2	Iteration #3	Iteration #4	Iteration #5
D	20.35	8.63	14.09	13.91	10.73
σ	17.74	7.31	7.28	9.22	7.50
A	47.71	50.96	56.68	53.99	61.82
Sp	46.93	50.09	57.91	55.32	64.59
Se	45.64	51.86	49.87	43.53	35.77
d	15.56	4.53	9.69	8.61	8.25

Also, partial anatomical maps, due to the cardiologist's interest in one particular area, lead to incompleteness of the activation wave. While constructing a more detailed map would be time consuming, operator input, where the cardiologist can correct or add features locally, is a feasible solution for better results. In this regard, the subsampling algorithm and the application of the presented method to sparse data provide guidance for the cardiologist in deciding which region needs more detailed information for a more accurate reconstruction.

In terms of termination point detection, while part of the error can be traced back to the path reconstruction inaccuracy, the learning feature vector itself can be enhanced with information such as wall thickness and estimated catheter tip motion at each point on the path, as described by [10]. The importance of additional information can be inferred from Table 2, where it is shown how different

activation paths led to different termination points. Starting with only a fifth of the full set of mapping points, the detection algorithm had limited electrical data gradients to differentiate between ablation and regular sites (high sensitivity and low specificity). With the addition of mapping points, the specificity increased.

Despite the expected benefit of the leave-one-out learning of tachycardia termination, the results in Table 1 do not support this method. The most numerous cohort of RA tachycardias does not have a high score in any of the accuracy, sensitivity, or specificity. This is probably due to the high variability in the set, but also because of the error in the first stage of path reconstruction. In fact, it can be inferred from Table 1 that the termination accuracy is inversely correlated with the mean distance to the CARTO points on the ground-truth path, i.e. the path reconstruction accuracy. This is also the reason why the single TCPC case, with a small error of path reconstruction, has the best accuracy and specificity result, despite not being able to learn from other TCPC maps.

On the computational side, the two-step method of reconstruction and learning can be easily integrated into a real-time solution. The tachycardia circuit detection runs in approximately 42.2 ms. The subject-specific RUSBoost classification runs in approximately 2.1 s, considering that the data base of the training model can be learned offline and only the test data needs to be labelled. Times were measured on an i7 CPU at 2.4 GHz with unoptimised Matlab code.

In conclusion, this paper presents a method for effective combination of graph traverse and ensemble learning classification algorithms for reconstructing macro-reentrant tachycardia circuits and identifying the site of most probable termination. It is based on the identification of the shortest path from the earliest to the latest activation time along the arrhythmia propagation curve. The anatomy was modelled as a graph with edges weighted by the propagation speed between two adjacent vertices and the conductivity of the tissue measured as local potential. After reconstructing the activation path, the point of most probable termination was sought. RUSBoost was applied in a leave-one-out ensemble learning framework, where the pattern of LAT-bipolar-unipolar voltage of typical termination points was learned.

Finally, both the activation reconstruction and the termination point detection were run on subsets of the original mapping points. This anticipates re-mapping guidance after ablation in order to verify the uninducibility of the ablated tachycardia. Moreover, the reconstruction from undersampled data can provide an optimal order of mapping points acquisition in similar anatomy.

References

1. Relan, J., Chinchapatnam, P., Sermesant, M., et al.: Coupled personalization of cardiac electrophysiology models for prediction of ischaemic ventricular tachycardia. Interface Focus **1**(3), 396–407 (2011)
2. Prakosa, A., Sermesant, M., Allain, P., et al.: Cardiac electrophysiological activation pattern estimation from images using a patient-specific database of synthetic image sequences. TBME **61**(2), 235–245 (2014)

3. Mitchell, C., Schaeffer, D.: A two-current model for the dynamics of cardiac membrane. Bull. Mat. Biol. **65**, 767–793 (2003)

4. Zettinig, O., et al.: Fast data-driven calibration of a cardiac electrophysiology model from images and ECG. In: Mori, K., Sakuma, I., Sato, Y., Barillot, C., Navab, N. (eds.) MICCAI 2013, Part I. LNCS, vol. 8149, pp. 1–8. Springer, Heidelberg (2013)

5. Zhu, H., Sun, Y., Rajagopal, G., Mondry, A., Dhar, P.: Facilitating arrhythmia simulation: the method of quantitative cellular automata modeling and parallel running. Biomed. Eng. Online **3**, 29 (2004). doi:10.1186/1475-925X-3-29

6. Cárdenes, R., Sebastian, R., Soto-Iglesias, D., Andreu, D., Fernández-Armenta, J., Bijnens, B., Berruezo, A., Camara, O.: Estimation of electrical pathways finding minimal cost paths from electro-anatomical mapping of the left ventricle. In: Camara, O., Mansi, T., Pop, M., Rhode, K., Sermesant, M., Young, A. (eds.) STACOM 2013. LNCS, vol. 8330, pp. 220–227. Springer, Heidelberg (2014)

7. Cignoni, P., Corsini, M., Ranzuglia, G.: MeshLab: an open-source 3D mesh processing system. ERCIM News **73**, 45–46 (2008)

8. Dijkstra, E.: A note on two problems in connexion with graphs. Numerische Mathematik **1**, 269–271 (1959)

9. Seiffert, C., Khoshgoftaar, T., Van Hulse, J., Napolitano, A.: RUSBoost: a hybrid approach to alleviating class imbalance. Trans. Syst. Man Cybern., Part A **40**(1), 185–197 (2010)

10. Constantinescu, M., Lee, S.-L., Ernst, S., Yang, G.-Z.: Multi-source motion decoupling ablation catheter guidance for electrophysiology procedures. In: Camara, O., Mansi, T., Pop, M., Rhode, K., Sermesant, M., Young, A. (eds.) STACOM 2014. LNCS, vol. 8896, pp. 213–220. Springer, Heidelberg (2015)